Retopology and Simplification of Reality-based Models for Finite Element Analysis

Marco Rossoni[1], Sara Gonizzi Barsanti[2], Giorgio Colombo[3] Gabriele Guidi[4]

[1]Politecnico di Milano, marco.rossoni@polimi.it
[2]Politecnico di Milano, sara.gonizzi@polimi.it
[3]Politecnico di Milano, giorgio.colombo@polimi.it
[4]Politecnico di Milano, gabriele.guidi@polimi.it

Corresponding author: Marco Rossoni, marco.rossoni@polimi.it

Abstract. Reality-based 3D techniques and Finite Element Analysis share the way the object under investigation is discretized. Although their purpose, the generation methods and the quality metrics are different, both of them ground on the concept of mesh. Unfortunately, a mesh derived from a reality-based technique are not suitable to be used in a finite element solver directly. This paper aims at comparing different methods to prepare computational mesh of geometries derived from non-contact reality-based technologies. A benchmark test object has been acquired with different devices, a triangulation laser scanner, a multi-stripe triangulation scanner and a digital camera, and post processed in order to fix artifacts. Then, two different decimation approaches have been used: a triangular simplification and retopology. The acquired geometry, before and after the simplifications, has been compared with a CAD model employed as reference: mean and standard deviation between the nominal and the acquired geometries have been tracked. Finally, a tensile test has been simulated making use of a general-purpose finite element analysis software and the results have been compared with the exact solution.

Keywords: Reverse Engineering, Laser Scanner, Structure from Motion, Retopology, Finite Element Analysis
DOI: https://doi.org/10.14733/cadaps.2020.525-546

1 INTRODUCTION

Reverse Engineering has been exploited for several purposes, e.g measuring and inspection[8], custom-fit design [12], cultural heritage [17]. Regardless the method or adopted technology, the result of this process is a 3D representation of the target, usually encoded in an unstructured faceted surface fashion (e.g. an STL file). Going beyond the mere visualization purposes and focusing on engineering products, prediction of

mechanical performances is often required, especially for items critical from a structural perspective. Finite Method Analysis (FEA) is a de-facto standard to evaluate mechanical performance, both in academia and industry. The FE method grounds on the discretization of a continuous domain into a set of elements and, when the domain is a 3D space, it is usually made through polygons. Unlike reverse engineering geometry representation, the computational grids requires a proper degree of accuracy, precision and reliability through the whole pipeline, from the acquisition of the geometry to the analysis of the final results. Unfortunately, the meshes derived from reverse engineering techniques are not suitable for direct use in FEA solver. Regardless the reverse engineering technology chosen, the standard pipeline requires the acquisition of the chosen object and the post process of the 3D model obtained to make it watertight and error free. The most important and thorny phase is the one related to the topological check of the 3D mesh and its simplification to obtain a proper model, suitable to be then translated in a computational grid for FEA. The problem is not new in literature [10, 16] but researches have been focused more on large items (e.g. buildings). Firstly, the order of magnitude of the relevant feature is different: concerning architectural items, small features, i.e. less than 1mm could be considered negligible. Secondly, similar works conducted so far don't evaluate FEA results systematically. Template-based reverse engineering has been also studied for mechanical parts [7, 8]: this methods assumes and make use of parametric CAD models as templates to fit and derive CAD models from tessellated surface. Instead, the rational behind this work assumes that the CAD geometry of the part being surveyed is not known a-priori.

This paper aims at comparing different methods to prepare computational mesh of geometries derived from non-contact scanning technologies. A benchmark case, i.e. a structural-steel parallelepiped, has been chosen in order to have complete control over the variables involved in the process (both during the reverse engineering and the FEA). The test object has been acquired with different devices, a triangulation laser scanner, a proprietary multi-stripe triangulation scanner and a digital camera, and post processed in order to fix artifacts. Once the tessellated surface is closed and error-free, two different methodology for simplification have been used: a triangular simplification and retopology. The simplification aims at reducing the number of triangles while maintaining the same geometry and dimensions: it allows to remove redundant information, reduce over-sampled geometry and make meshes easy to handle during the post processing phase. The acquired geometry, before and after the simplifications, has been compared with the reference model (i.e. a 3D geometry created using CAD geometric primitive): mean and standard deviation between the baseline model and the acquired geometries has been tracked. Finally, a tensile test has been simulated making use of a FEA software and the results have been compared with the analytic solution.

The terminology and vocabulary relative to CAD, FEA and reverse engineering domain is sometimes overlapping: the term *mesh* is used extensively among them but with different meaning. For the sake of avoiding misunderstanding, we define *tessellated surface* the representation of a surface via polygons (i.e. mesh in CAD and reverse engineering domain, usually encoded in stl file), while we call *mesh* the computational grid (i.e. the mesh in the sense of FEA).

The paper is organized as follow. Section 2 describes the theoretical background of 3D reality-based techniques, the reverse engineering process and the best practices for topology check of the acquired 3D data. Section 3 describes the survey process indicating for each technology used the specifications of the instruments and the accuracy achieved. Section 4 is related with the description of two different process for simplifying an high- resolution 3D tessellated surface. Finally, section 5 regards the FEA and the discussion of results.

2 BACKGROUND

Reverse engineering aims at taking something as a software, an object or a device apart to analyze its functionality and with the intention of constructing a new object or device starting form the initial one [25].

Given a physical object, the reconstruction of its geometry in a digital fashion is referred as Reverse Engineering in Computer Aided Design area. Historically, reverse engineering models has been employed when

(i) product design involves physical prototype; (ii) re-manufacturing of part whose design data have been lost; and (iii) measurements to determine deviation between design and manufactured product [15].

Three dimensional digitization (also known as sampling or acquisition) refers to the first step of the workflow in which the target is converted in the digital world in the form of Point Cloud (PC). It can occur with or without contact. In this work, non-contact technologies (reality-based techniques) are taken into account: among them, two different triangulation based 3D laser scanner and photogrammetric reconstruction have been considered.

Active systems, the category laser scanners belong to, operate regardless of the light and texture of the object to be detected as they modify the exterior appearance with suitably coded light and the PC is obtained through as a series of three-dimensional coordinates. All scanning systems operate through an almost automatic process through which they can acquire a large amount of points per second, even in the order of one million. Triangulation laser scanners are based on the principle of triangulation that allows to obtain the measurement of the cathetus of a rectangle triangle, knowing the measure of the second cathetus and the angle between the known cathetus and the hypotenuse. Hence, the geometric principle of the triangulation system requires a point on the surface of the object, a projector and a camera, arranged in such a way as to form the three vertices of a triangle in the space. Known three parameters (i.e. the measurements of the base between the projector and the camera and those of the receiving corner and the projection angle) it is possible to obtain, by simple analytic steps, the size and shape of the triangle but, above all, the distance from the object.

Photogrammetry can be define as "the process of deriving (usually) metric information about an object through measurement made on photographs of the object" [24]. The starting point for building the fundamental relationships of photogrammetry is the prospective projection: a point A projected on a projection plane creates a trace A' and the two points are called homologous points. Once the position in space of point A is known, it is possible to calculate its position on a projection plane at a certain distance from the perspective centre. However, if a single point can be calculated on a single image plane, it is not possible to do the opposite, that is, to calculate the coordinates of one point in space from one image. For this reason, photogrammetry predicts that at least two images of the same scene, taken from two different points of view, have to be used. Measuring the position on the image of the projection A' resumed from two different points of view it is possible, by using the collinearity equations, to calculate the distance from the point A to the camera in three dimensions [24]. Simplifying, thanks to a couple of measurements in a 2D space (images), a measure in 3D space is known. The collinearity equations allow to calculate the coordinates of the object in space, by using at least a couple of images where the same point is visible. The use of two images is necessary because only having two views of the same object can be calculated the three spatial unknowns of the object itself. The process calculates the external orientation of the camera, meaning 6 parameters related to the spatial position and the orientation of the camera coordinate system with respect to the global coordinate system of the object and the internal parameters defined by the focal length of the camera, the coordinate in the image of the principal point and the parameters related to the different distortion of the lenses. The mathematical model at the basis of the photogrammetric restitution process is defined as a collinearity model that is solved by the principle of "Bundle Adjustment" (also called "projector block compensation") and using the minimum square process [23]. In this paper, Structure from Motion (SfM) technique has been used. It extends the capabilities of the traditional photogrammetry by determining internal camera parameters, the camera position and its orientation automatically, without the need for a predefined set of ground control [30]. In this work, Agisoft Photoscan has been used: it is one of the most used software implementing SfM pipeline.

Regardless the technology, reality-based techniques usually deliver as raw data a 3D point cloud. The main difference is that laser scanning results are metric while photogrammetry/SfM needs metric reference to scale the 3D data. Then, the first rough tessellated surface is obtained fitting the point cloud. Methods and algorithm to undertake data processing has been extensively studied: usually, the scope is to obtain an error-free, closed tessellated surface. Triangular tessellated surface are defined by a series of triangles which barycenter describes a linear surface representation. A tessellated surface can be described by a set of vertices

$V = \{V_1, ..., V_v\}$ and a set of triangles connecting them $F = \{f_1, ...f_F\}, f_1 \in VxVxV$ even if is more efficient to define the triangular tessellated surface with the edges of the polygons since the connectivity occur by the triangles edges $\epsilon = \{e_1, ...e_E\}, e_1 \in VxV$ [6]. Actually, a bunch of algorithms have been proposed in literature for point cloud to surface reconstruction [3]: each of them pursues a defined goal, addresses specific problem and has its own limitations. The non-uniform point sampling, noise, sampling inaccuracy and scan misregistration make the reconstruction of surfaces from oriented point cloud difficult. There are different approaches to deal with these kind of PCs. The meshing algorithm can exactly interpolate all or most of the points: notable examples are the Delaunay triangulations, the alpha shapes, or the Voronoi diagrams. Doing so with noisy data, the resulting surface is often rough and irregular and the triangulated surface is smoothed or refit to the points in subsequent processing. Other methods, global or local approaches, directly reconstruct an approximating surface. Global fitting methods define the implicit function as the sum of radial basis functions centred at the points. Local fitting methods consider subsets of nearby points at a time. A simple scheme is to estimate tangent planes and define the implicit function as the signed distance to the tangent plane of the closest point. Finally, Poisson reconstruction creates very smooth surfaces that robustly approximate noisy data and it is well known for their resilience in the presence of imperfect data [22]. Specific algorithms and approaches have been then proposed to address specific issues in reverse engineering and engineering problems, for example algorithm for automatic and feature-preserving hole-filling in a CAD mesh model [1] or framework for 3D model reconstruction [29]. They provide useful means to solve specific issue but lacks of generality. In this work, we opted for the Screened Surface Poisson reconstruction algorithm because it is one of the most robust, general-purpose and widespread implementation.

Before being suitable for any scope, the tessellated surfaces should be checked against topology errors. In fact, most applications using 3D models require such models to be geometrically and visually accurate and free from noise, outliers and missing data or holes. Not only such errors make the models unusable for documentation or reproduction but also create unpleasant visual experience. Talking about tessellated surface and mesh, topology refers to the layout of the grid, so how nodes and elements are connected to each other. A polygonal tessellated surface consists of three kinds of elements: vertices, edges, and faces which information are described by tessellated surface connectivity and tessellated surface geometry. A topological metrics describes the relations among tessellated surface elements: a good topology for a 3D model means avoiding self-intersecting polygons, holes, duplicated vertices or faces, non-manifold faces. A tessellated surface is a manifold if each edge is incident to only one or two faces and the incident faces to a vertex form a closed or an open fan. Furthermore, two adjacent faces needs compatible orientations. Any abrupt change in this relationship is considered a topological error, like for example flipping the normals of two adjacent polygons.

Reality-based 3D models are usually referred to as high-resolution models, that results in polygonal surfaces with an high number of elements. Dealing with them could be challenging and, most times, the density of the elements does not make the 3D model better. A simplification or decimation process consists in reducing the number of the triangular elements while keeping the resulting surface as similar as possible to the the initial high-resolution tessellated model. The simplification/decimation algorithms transforms a given polygonal tessellated surface into another with fewer faces, edges, and vertices reducing the complexity of the high resolution tessellated surface. The simplification process is usually controlled by a set of user-defined quality criteria that can preserve specific properties of the original tessellated surface as much as possible (e.g., geometric distance, visual appearance , etc). There are different approaches, the majority of which involves the degradation of the tessellated surface to reduce the number of polygons [14]. The Vertex decimation removes vertices and the adjacent faces and, for each step of the simplification, the vertices are evaluated taking into account their importance, the adjacent faces are deleted and the resulting hole triangulated [26]. The sequential optimization process guides the removal of points from the triangulation leading to a gradual increase of its overall approximation error and represents a derivation from the Delaunay Pyramid method first proposed in [13]. Another decimation approach is based on the energy function optimization [19]: this class of algorithms assign an energy function to the number of nodes, the approximation error and the regulatiry of

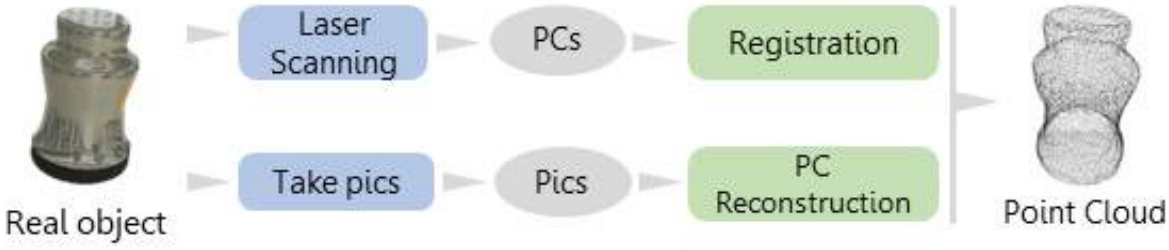

Figure 1: Conventional pipeline of reverse engineering in CAD: from real object to Point Cloud (PC).

the mesh. The objective is then to minimize the energy: it produces high quality results but the computational cost hugely increases [27]. Other example of simplification approaches are vertex clustering adn face Clustering [27]. In this work, a multi-resolution vertex decimation algorithm has been used that optimally reduces the number of triangulation vertices. It allows the user to specify just a minimum set information (e.g. tolerance between the reduced triangulation and the original one, or minimum number of polygon).

In this work, beside the traditional decimation, we want to investigate the use of retopology. It refers to the informal name of a class of algorithms aiming at re-meshing a surface in a uniform shape elements, either triangular or quadrilateral. The terms retopology comes from the world of 3D computer animation [5]. To make the models more suitable to be animated, 3D artists make use of quad-based topology to take advantage of clean tessellated surfaces and edge-loops. With quads, it is easier to add or manipulate edge loops and to obtain a smoother deformation. A quadrangle tessellated surface (or quad-dominant) is mainly made by quads and some unavoidable triangular polygons in case of complex geometry. Quad-based topology consists of rows and columns, a simple topology and an outcome easily to be subdivided, while a model with triangle-based topology can product sharp angles that can affect the design of a tessellated surface. The quadrangular method samples the original tessellated surface at a spatial resolution lower than the original with a degree of accuracy higher than a triangular tessellated surface, because it preserves the global geometry of the original tessellated surface, re-defining its topological structure [2]. Quad tessellated surfaces are then preferred in the Finite Elements Analysis since they reduce the errors and the number of superficial elements that constitute the model, compared with triangular tessellated surface [4].

3 SURVEYS AND AS-IS 3D MODELS

The section provides a brief description of the instruments employed and presents how surveys have been carried out for repeatability purpose. The survey phase goes from the acquisition of the real object to the achievement of a point cloud (Fig.1). In the case of laser scanners, the point cloud is the registered point cloud, that is when all the single scanned point sets have been aligned properly. Then, how tessellated surfaces have been interpolated from the point cloud will be exemplified: selected algorithms and procedures are pointed out along with the parameters chosen (Fig.1). Finally, the comparisons among the scanned and the nominal object (i.e. CAD model of the parallelepiped) is presented to promote discussion about an optimal and straightforward way to obtain a proper tessellated surface.

The test object for this project is a structural steel parallelepiped whose dimensions are 50x50x120 mm. In addition to its simple geometry, the test object is relevant for engineering application due to its sharp edges: digitization technologies struggle to accurately detect those feature leading to problems during the survey and topological errors in the final 3D tessellated surface. The problem is very well known and it is inherently coupled with the physics principles exploited by laser scanning: sharp edges are now reconstructed by hand during post-processing, bringing to geometrical errors not be entirely negligible for engineering application.

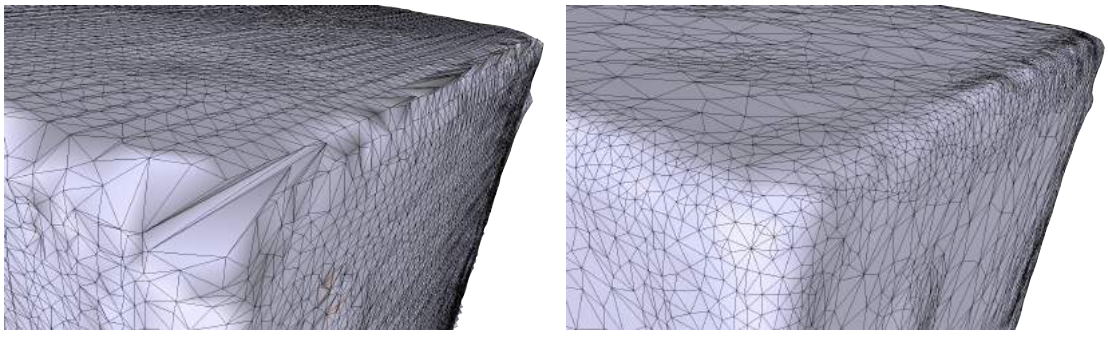

(a) (b)

Figure 2: Acquisition of sharp edge and corner by laser scanner: (a) noise and artifact: (b) round.

Technology	Model	Configuration	Accuracy $[mm]$	Precision $[mm]$	Resolution $[mm]$
Laser	Konica Minolta Vivid 9i	tele-lens distance $\sim 650mm$	0.08	0.043	0.176 - 0.052
Laser	Next Engine 2020i	default	0.3	-	-
Digital camera	Canon 5D Mark II	36 x 24 mm sensor 20mm focal length 641 μm pixel size	-	-	0.144

Table 1: Technical specs and configurations of the digitization tools.

In the area close to a sharp edge, artifacts, noise (Fig.2a) and/or round features (2b) are usually gathered depending on the accuracy of the instrument: the former is known as laser scattering [18] and affects laser-based technologies, the latter spreads all over non-contact digitization technologies. In the comparison sections (Sec.4), further details about them will be discussed. Every technology has its own limitation about material suitable to be acquired, and so on. In order to avoid light reflections, the object has been made opaque by white paint. The coating is few μm thin, hence the geometrical alteration will be neglected. Furthermore, since rich textured surfaces are needed for photo-based process, targets have been applied on the faces of the parallelepiped to make them different from one another (Figure 4). Those targets make the alignment and registration processes easier, both with laser scanners and digital camera. The survey has been carried out with different devices whose technical specs and configuration are reported in Table 1.

The Minolta Vivid 9i is a triangulation laser scanner, equipped with a tele-lens: considering the dimension of the object and the distance of scanning, its estimated uncertainty is 43 μm. The scanner employs laser-beam light sectioning technology to scan work pieces using a slit beam. Light reflected from the work piece is acquired by a CCD camera, and 3D data is then created by triangulation to determine distance information. The laser beam is scanned using a high-precision galvanometric mirror, and 640x480 individual points can be measured per scan. The parallelepiped was surveyed with 17 scans, moving the object in front of the scanner in order to have the entire surface covered. InnovMetric Polyworks has been used for the alignment considering the circular black on white markers placed on the surface and, at the end of this phase, the mean standard deviation was 0.05mm, close to the uncertainty of the instrument.

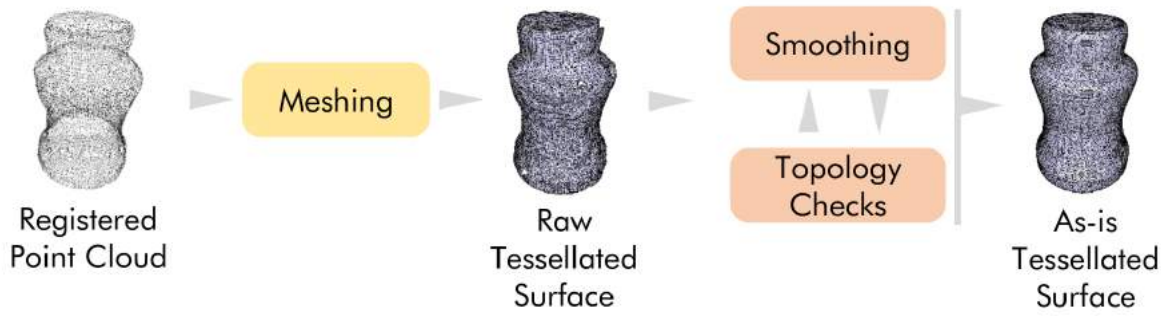

Figure 3: Conventional pipeline of reverse engineering in CAD: from point cloud to tessellated surface.

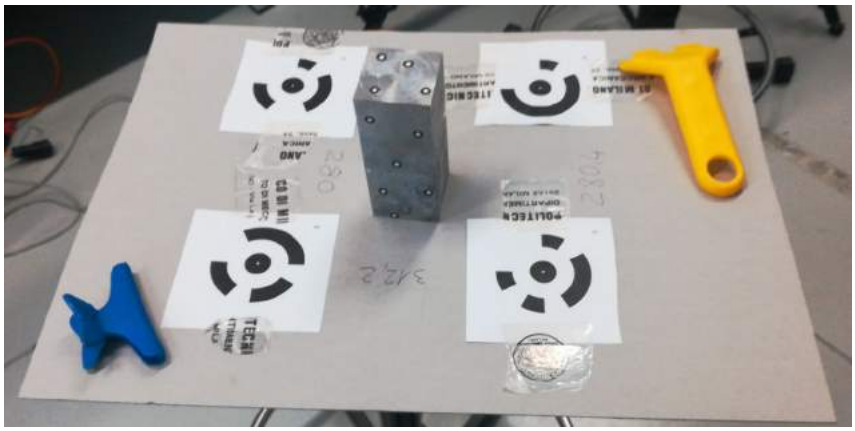

Figure 4: Structure from Motion setup

The second scanner used for the survey was a Next Engine 3D laser scanner that uses a multistripe triangulation system with twin array of four solid-state lasers with nm wavelength and 3.0 Megapixel CMOS image sensors [31]. The acquisition of the test object was performed placing the parallelepiped on the proprietary turning table, first on the short side and then on the long side to acquire the entire surface. The alignment of the different scans was performed with InnovMetric Polyworks in order to follow the same procedure with the two different laser scanner acquisition. The mean standard deviation at the end of the alignment phase was 0.4mm, acceptable related to the uncertainty of the scanner.

The use of a twin array of four vertical lasers, scanning from right to left, may have increased the noise and the slipping of 3D points around the corners of the object. During the survey phase, the scans visible in the proprietary software ScanStudio presented a jagged surface especially around the corners when the test object had its planar side in front of the scanner. Because of this noise, during the alignment of the scans, the corners and the sharp profiles of the model resulted smoothed and presented several non-manifold and self-intersecting triangles.

The third survey has been carried out with a Cannon 5D Mark II digital camera, equipped with a 20 mm lens. Figure 4 shows the setup with photos have been shot: targets and auxiliary objects have been placed there to make the alignment and scaling procedure easier. As resolution metric, the ground sample distance (GSD) has been considered, that is how much each pixel accounts in the real word. Equation 1 shows how GSD has been estimated for the camera at hand. Since, the pixels are square, the GSD along the image height

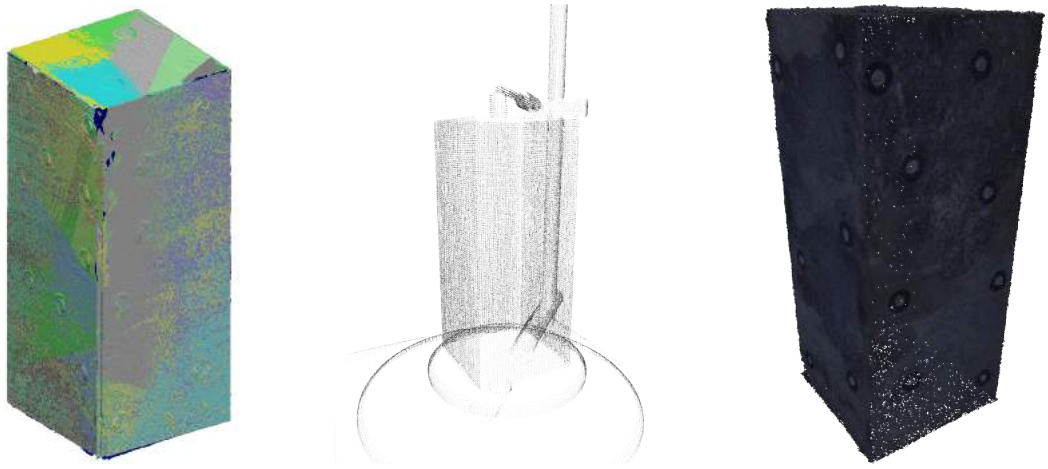

(a) Minolta 9i Vivid, software: Polyworks

(b) Next Engine 2020i, software: NextEngine Studio

(c) Cannon 5D Mark II, software: Photoscan

Figure 5: Registered point clouds as obtained by Polyworks, NextEngine Studio and Photoscan.

and width are the same. In our survey GSD is 0.144 mm/px.

$$GSD = \frac{ShotDistance \cdot PixelSize}{FocalLenght} = \frac{450mm \cdot 0.00641mm/px}{20mm} = 0.144mm/px \tag{1}$$

The construction of the dense point cloud has been performed with Agisoft Photoscan. The test objects has been surveyed through 68 images, acquired in RAW data and then post-processed and exported in jpeg format in Lightroom to control and correct white balance, light and shadows. This passage is mandatory since Photoscan does not open RAW data. The survey was done placing the object on a table and moving the camera around it. Due to environmental light, a tripod for the camera was used since the settings of the camera were ISO 400 to avoid blurring images and aperture 7.1. With these settings, the time of shooting was too long for taking the images by hands. For the acquisition phase and to help the alignment of the images, since the test object has little texture and a simple geometry, the circular, black on white markers placed on the surface have been used. The images were imported in Agisoft Photoscan and aligned using the High parameter, that uses the full resolution of the images. From the obtained sparse cloud, a dense cloud of almost 4 million points have been produced using also the High parameter. The scaling of the point cloud was performed placing a square plate with four proprietary markers at known positions under the test object.

As shown in Fig.3, the next steps in the pipeline is generation a tessellated surface from the registered point cloud. Even if both InnovMetric Polyworks and Agistoft Photoscan are able to generate tessellated surfaces, only the point clouds have been saved: since they are proprietary software, it does not let the user full control over meshing and smoothing algorithms. For this reason and to keep the three surveys comparison independents from the meshing algorithm, the tessellated surfaces have been generated using Meshlab [11], adopting the same pipeline for each of the three point clouds. First, the normals for the point set have been computed with a k-nearest based algorithm: for each point, a plane fitting n neighbour points is computed and the normal is stored. This algorithm is among the predefined filters of Meshlab and the number of neighbors used to estimate the normal (n) has been set to 100. Then, Screened Surface Poisson reconstruction algorithm [22], already exposed by Meshlab, has been used to create the tessellated surface. The parameters have been left as default except for the "reconstruction depth". It refers to the maximum voxel grid resolution used for

Model	Vertices [x1000]	Faces [x1000]	Alignment Residuals [mm]	Geometric Error μ [mm]	σ[mm]
Minolta	229	453	0.05	0.21	0.15
Next Engine	110	220	0.4	0.19	0.27
Canon 5D Mark II	3623	1327	-	0.07	0.22

Table 2: As is tessellated surfaces. The alignment residuals refer to the standard deviation estimated at the end of the alignment.

the surface reconstruction: as a rule of thumb, the more the point cloud is noisy, the more this value has to be raised. The value of 12 has been set for all the point clouds. Another way the algorithm relaxes the noise is by acting on the screened term (interpolation weight in Meshlab): noisy point clouds require low screening that, however, entails smooth reconstructions and degradation of detailed features. It is difficult to find a smoothing parameter that simultaneously preserves detail and avoids the formation of spurious geometry: given this dependency between noise and detailed feature, the authors preferred to keep the settings to preserve as much as possible the details and smoothing afterwards. For this reason, a Taubin smoothing filter [28] has been applied: it was implemented in order to avoid typical shrinkage phenomena that affect, for example, laplacian smoothing. For this reason, it suites well for our scope, where the preservation of the geometrical dimensions and features is essential. It approximates an ideal low-pass filter to produce a smooth non-shrinking surface: firstly, a laplacian operator (λ) smooths the surface (with shrinkage) by some positive value and then a laplacian with a negative parameter (μ) is applied. The magnitude of (λ) should be slightly larger than (μ) to contrast the tendency to shrink of the laplacian smoothing .Default values for the parameter λ and μ, 0.5 and -0.53 respectively, have been used.

The quality check of the topology was done in Meshlab as well, applying several filters to clean the data: (i) Remove duplicate faces/vertex; (ii) Remove faces from Non Manifold edges; (iii) Remove unreferenced vertex; (iv) Remove zero area Faces; and (vi) Select and cancel non Manifold Edges/vertices. The aims is at obtaining a clean, error-free topology, watertight tessellated surface and, eventually, obtaining a closed superficial tessellated surface to be filled up with element to discretize the enclosed volume, suitable for FEA.

Table 2 reports the number of vertices and faces obtained for the three surveys and the related alignment residuals. All of them are in line with the uncertainty of the tools. In order to verify the acquisitions, a comparison between the generated tessellated surface and the nominal parallelepiped 50x50x120 mm has been performed. The cloud-to-mesh distance with the built-in function of CloudCompare 2.6 has been used for all the comparison through this paper. Taking as reference the nominal parallelepiped, the mean (μ) and standard deviation (σ) of the signed distance are shown in Table 2. The tessellated surface resulting from the SfM process is the most accurate in terms of geometric average deviation from the reference model. It shows the best fit when compared with the nominal model, and this is confirmed by the mean and standard deviation obtained. These results are quite surprising, since laser scanner are well known for best accuracy over the photogrammetry based approach, especially on reflective, planar and little textured objects. The less noise of the as-is SfM model is one of the reason for it. Since the process uses images, if the survey is performed in a proper way, the errors and the slips of the 3D points on the corners of the test object is less noisy than in the one obtained by laser scanning. As expected, the greatest errors occurs near the corners and along the edges of the parallelepiped 6, especially for the two laser scanners. These models will be the reference for the following simplification and retopology phase (Figure 7).

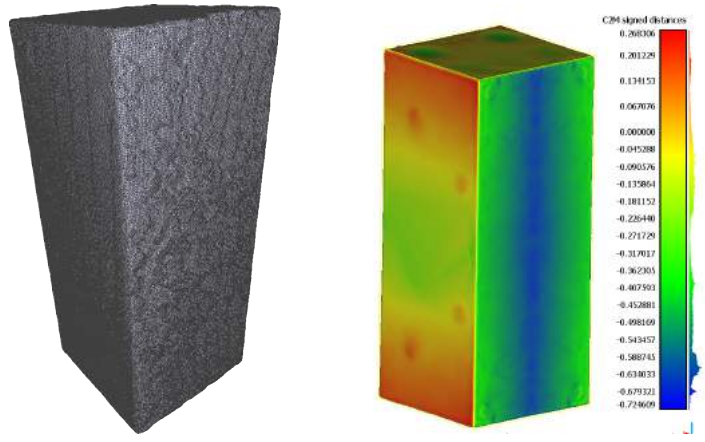

(a) Minolta.

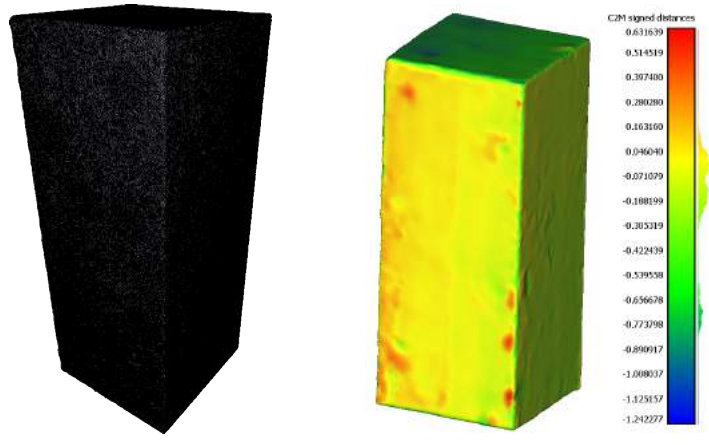

(b) Next Engine.

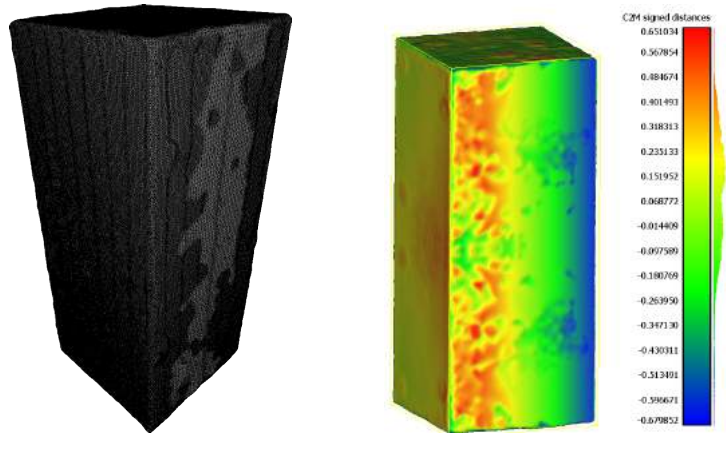

(c) Structure from Motion.

Figure 6: Tessellated surface and relative comparison with the nominal parallelepiped for (a) Minolta laser scanner, (b) Next Engine laser scanner and (c) Structure from Motion.

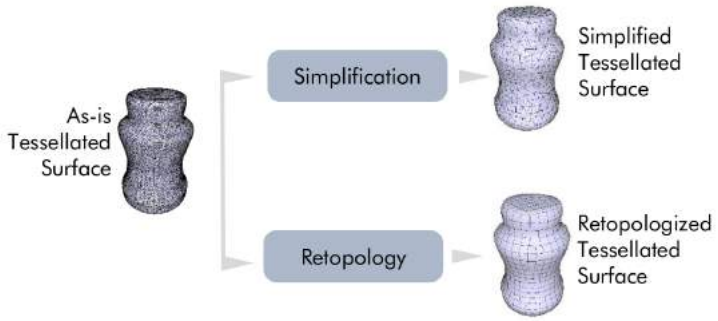

Figure 7: From the tessellated surface to the simplified and retopologized tessellated surface.

4 SIMPLIFICATION OF THE TESSELLATED SURFACES AND CREATION OF VOLUMETRIC MODELS FOR FEA

Reality-based models have usually extremely high resolution: the density of the vertices are sampled regardless the real topology of the surface, consequently large number of points are used to represent even flat surface. Moreover, the tessellated surface is affected by the unavoidable noise of the measurements, that last even after the smoothing process. Reducing the number of triangle and changing their shapes to quadrangles allow the tessellated surface to be easily handled and, likely, to reduce the number of the artifacts while retaining its global geometric properties. As decimation approaches, the triangular simplification and the retopology have been pursued in this work: the starting models are the *as-is*tessellated surfaces previously obtained (Fig.7). Polyworks IMCompress module, which implements a vertex decimation algorithm, has been used for triangular simplification. The retopology has been performed with Instant Meshes [20], which implements the Instant field-aligned approach based on a local smoothing operator[21]. It is a valuable methods to perform retopology because it naturally tends to create sharp feature from edges without the need to adjust any parameters, it accepts almost any surface representation (point clouds, range scans and triangle tessellated surface). The algorithm solves two global problems: estimation of the alignment of the edges of the new tessellated surface and element placement. The main limitation regards the introduction of singularities that, however, can be fixed afterwards. The algorithm has been exposed by Instant Meshes which permits to correct the superficial distribution of the elements, in order to have a better organization of the geometry. The first step uses an orientation field that guides the alignment of the edges in the final tessellated surface. The second step computes a local, per-vertex parametrization that matches the orientation field [21].

An optimal decimation process works towards getting the minimum number of polygons/vertices without changing the accuracy of the overall model. Of course, removing triangles affects the geometry of the model, hence a trade-off between accuracy and resolution should be pursued. Polyworks IMCompress permits two different triangular simplifications settings: the first imposes the maximum deviation allowed between the simplified and the non-simplified tessellated surfaces while the second specify the target number number of polygons. Since Instant Meshes suggests a target vertex count, it has been taken as initial guess: the software proposed 14, 40 and 7 thousand faces for Minolta, Next Engine and SfM as-is models respectively (Table 3). With those targets, the retopology as been performed and all the geometries have been checked again: this comparison aims at measuring the maximum geometrical deviation between the as-is models and the new retopologized surfaces. As reported in Table 3, the maximum deviation remains below 0.06 mm for all the models. On the left of Figure 8b, 9b, 10b, the resulting meshes are reported for the Minolta laser scanner, Next Engine laser Scanner and the Structure from Motion respectively. Then, the triangular simplification has been run for each model (the input is, again, the as-is tessellated surface) imposing a number of target polygon equal to the one suggested by Instant Meshes. In this way, the same decimation ratio has been applied and

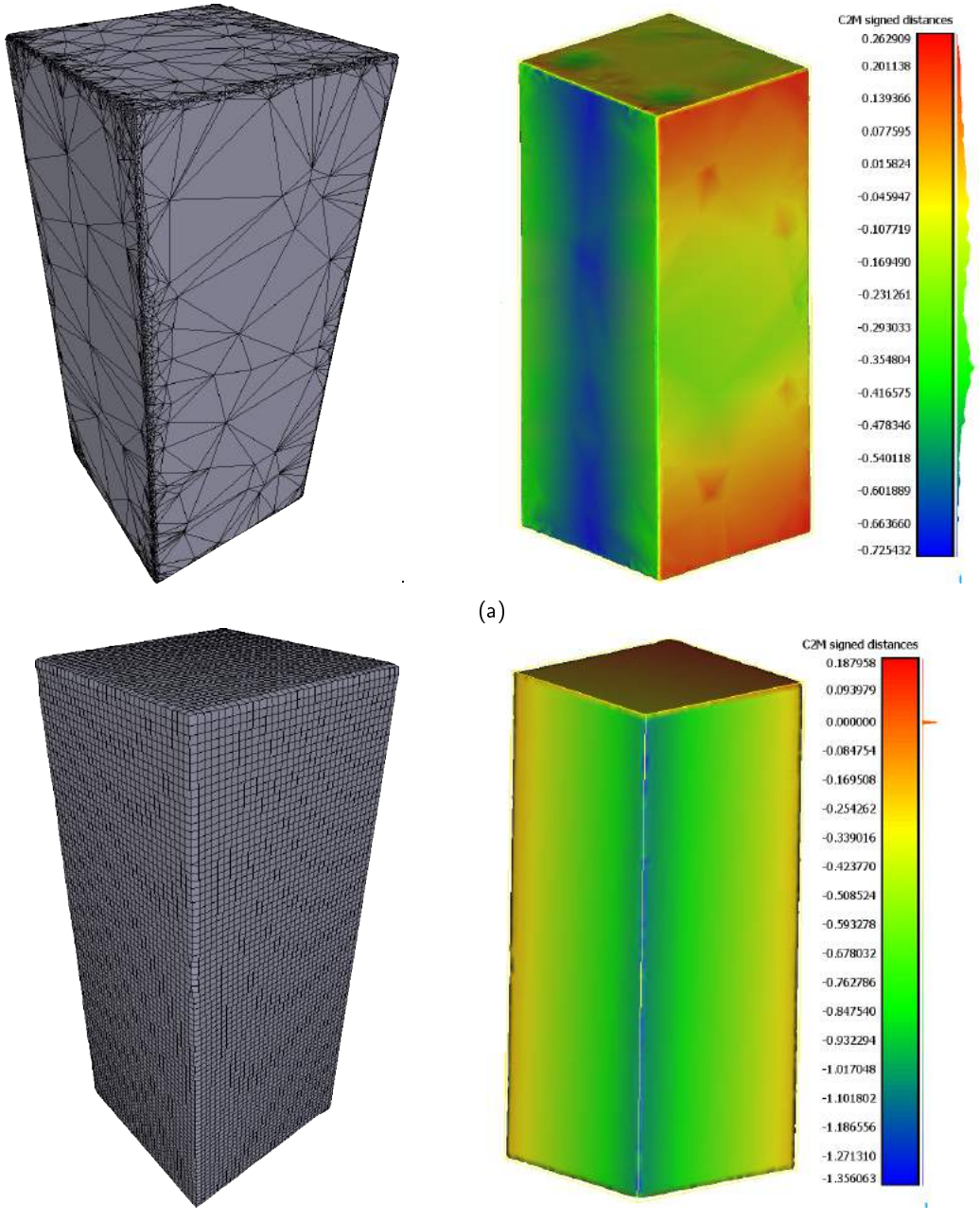

Figure 8: Mesh (on the left) and heat map (on the right) of the comparison with the nominal parallelepiped for (a) the simplified and (b) retopologized models acquired by Minolta laser scanner.

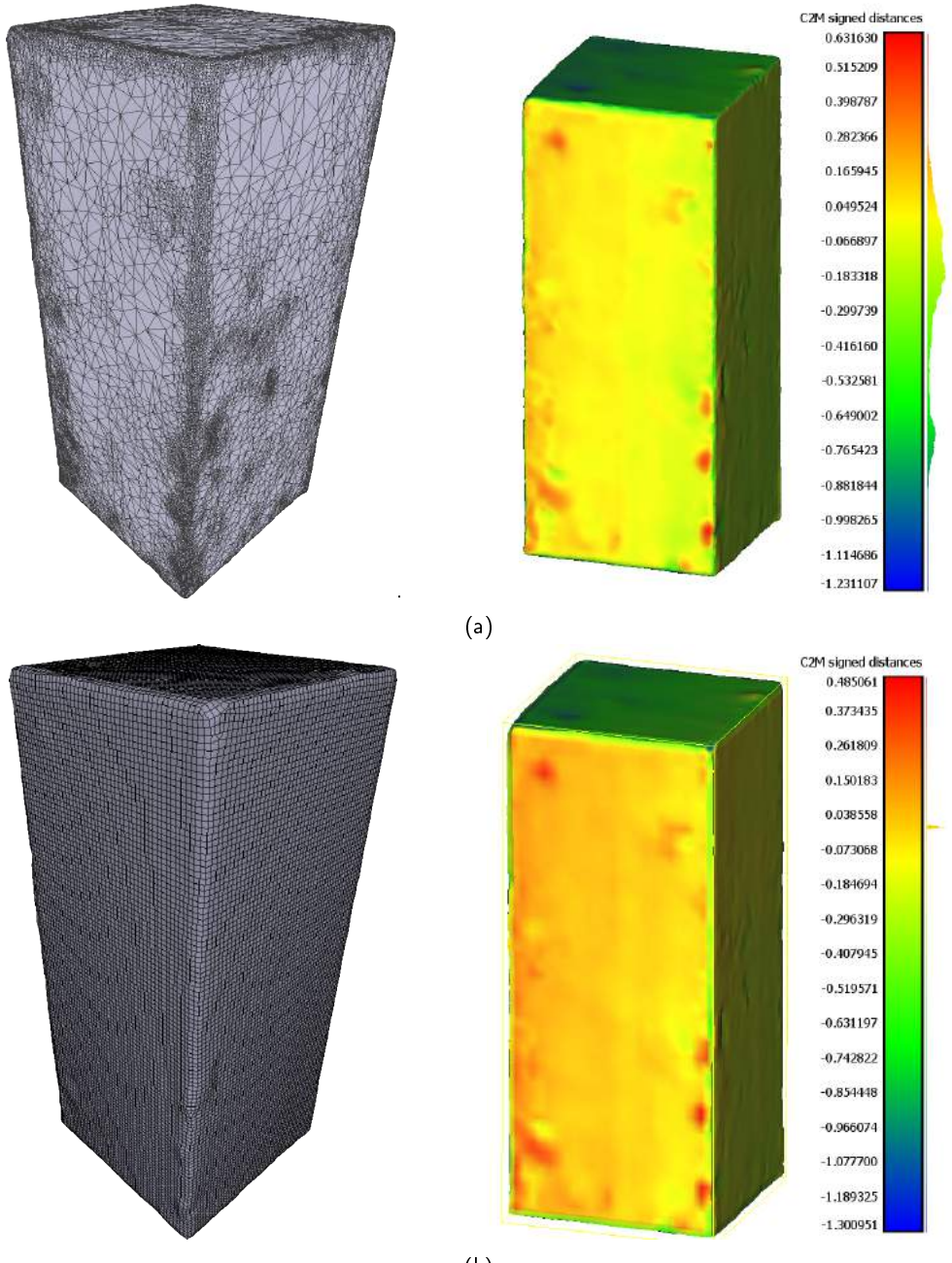

Figure 9: Mesh (on the left) and heat map (on the right) of the comparison with the nominal parallelepiped for (a) the simplified and (b) retopologized models acquired by the Next Engine laser scanner.

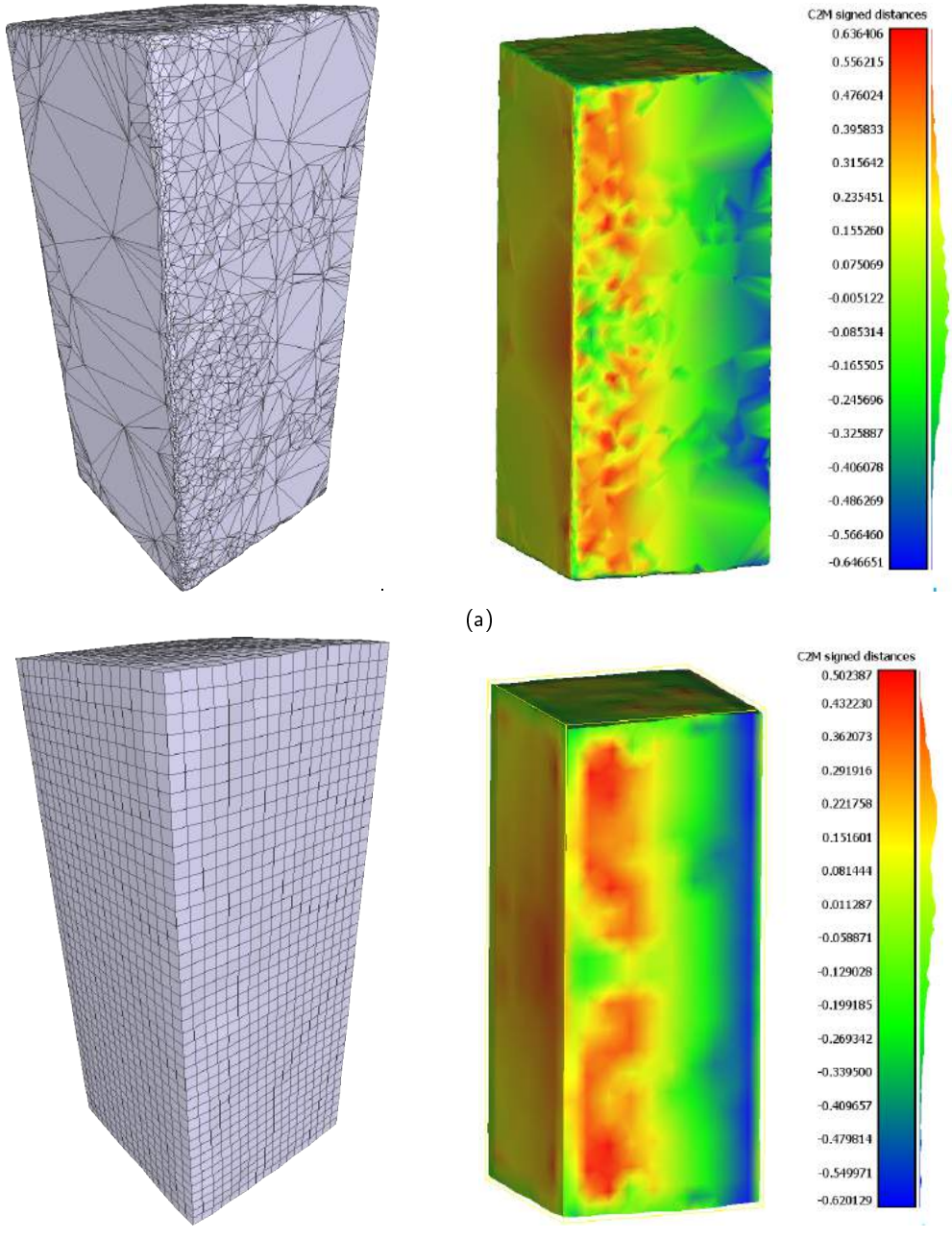

Figure 10: Mesh (on the left) and heat map (on the right) of the comparison with the nominal parallelepiped for (a) the simplified and (b) retopologized models acquired by Structure from Motion.

Model	Faces [x1000]		Geometric Error Reference: nominal parallelepiped [mm]		Max Deviation Reference: AS-IS model [mm]	
	Simp	Reto	Simp	Reto	Simp	Reto
Minolta	14	14	μ = -0.197 σ = 0.254	μ = -0.115 σ = 0.250	0.07	0.05
Next Engine	54	55	μ = -0.248 σ = 0.317	μ = -0.189 σ = 0.272	0.06	0.06
Canon 5D Mark II	7	7.3	μ = 0.009 σ = 0.221	μ = 0.066 σ = 0.217	0.05	0.05

Table 3: Number of faces, mean (μ) and standard deviation (σ) of the geometric error (mesh-to-cloud signed distance) between each model and the nominal parallelepiped, maximum distance between each model and its relative as-is version for triangular simplification (Simp) and retolopology (Reto) approach.

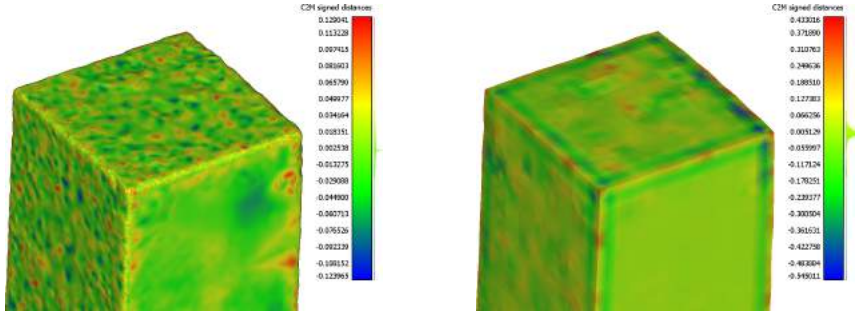

Figure 11: Close-up of the mesh-to-cloud signed distance between the as-is and triangular simplified surfaces (on the left) and the as-is and retopologized surfaces (on the right) for the SfM models.

the comparison between the two approaches of decimation will be more consistent. On the left of Figure 8a, 9a, 10a, the resulting meshes are reported for the Minolta laser scanner, Next Engine laser Scanner and the Structure from Motion respectively. The maximum geometric difference, as well as the number of faces for each model, are reported in Table 3. A relevant information is that the three photogrammetric models, the *as-is*, the triangular simplified and the retopologized one didn't show any topological error, so no operation was needed in Meshlab.

On the right of Figure 8, 9, 10, a set of heat maps represents the distribution of distance of each surveyed model from the nominal parallelepiped. As expected, the errors increase getting closer to the edges. Table 3 reports the mean (μ) distance and its standard deviation (σ) for each model. As general trend, the accuracy of the models is slightly affected by the decimation procedure in terms of accuracy of the model when compared to the nominal parallelepiped: it can be noticed that the error introduced by the retopology is, generally, less than the on caused by triangular simplification. However, the retopology allows a more even distribution of the element that, consequently, results in a more uniform and smooth error distribution. Furthermore, thanks to the feature preservation capability of the instant field-aligned algorithm, the tessellated surface close to sharp edges strongly improve, as shown in Figure 11 for the SfM derived model (laser scanners models shows the same pattern).

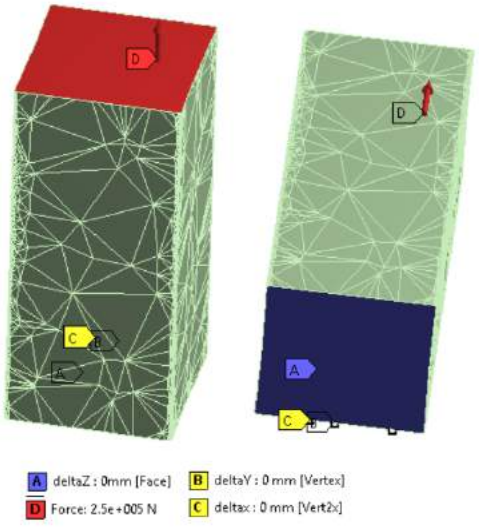

Figure 12: Boundary conditions and load applied in the FEA. The same configuration has been used for each model here reported.

5 FINITE ELEMENT ANALYSIS SETTINGS AND RESULTS

A tensile test has been simulated using a general-purpose FEA software, i.e. Ansys Mechanical R19.2. This simple test allows the results to be compared with a theoretical solution. The parallelepiped is supposed to be fixed and loaded with 100 kN (traction), at the bottom and top side respectively. Given that the cross-section area is 2500 mm^2, the tensile stress is 100 MPa constant: this stress is the reference value.

The FE models have been prepared in the same way for all the 3D models. In order to avoid singularities due to over-constrained elements at the base, three different boundary conditions has been applied (Fig. 12): (i) zero-displacement along the axis of traction (i.e. Z axis); (ii) zero in-plane (i.e. X-Y axis) displacement of one node; (iii) zero in-plane (i.e. X-Y axis) displacement of another node. The tessellated geometry has been imported within the meshing software and it is directly converted in the surface mesh while two different approaches for the generation of the volume mesh has been adopted. For the triangulated surfaces (i.e. the as-is and the simplification 3D models), tetrahedral volume mesh has been generated. The Advancing Front Tetra algorithm has been used to fill the internal volume of the as-is and simplified models: it is a bottom-up methods, hence the volume mesh is generated from the surface mesh without interfering with it. Instead, an hex-dominant algorithm has been used for the retopologized model: in this case, the quadrangular surface mesh has been specified as input for the volume mesh. The global seed (i.e. element side length) has been initially set equal to the smaller element on the tessellated surface. To verify the independence of the results from the mesh resolution, the global seed has been then halved: in all cases, the results have kept unchanged. The chosen element order is quadratic and the aspect ration has been taken as metric to check the mesh quality: it is defined as the ratio of the shortest length of the element to the longest length of the element. This value should be as close to 1 as possible and values in the range 1 to 3 are usually acceptable, while above this threshold should be treated with caution[9]. Moreover, the percentage of element whose aspect ratio is greater than 3 should be less than 5% [9]. These are guidelines that give reasonable account to consider the FEA results accurate. This approach allows us to keep unchanged the geometric characteristics of the tessellated surface. Table 4 reports aspect ratio values and percentage of element exceeding the value of 3: as can be notice, all the meshes are below the imposed threshold.

		Normal Stress [MPa]		Deviation from reference	Aspect Ratio		
		μ	σ	%	μ	σ	% > 3
Konica Minolta Vivid 9i	as-is	102.3	1.3	2.3	1.9	0.65	2.1
	simplified	102.2	2.1	2.2	3.0	2.29	3.4
	retopology	102.2	0.8	2.2	0.8	1.9	0.47
Next Engine 2020i	as-is	99.7	5.4	0.3	2.44	0.8	4.0
	simplified	100.2	5.1	0.2	2.42	0.89	4.3
	retopology	99.6	2.4	0.4	1.92	0.7	1.1
Canon 5D Mark II	as-is	99.6	5.0	0.4	1.8	0.45	1.6
	simplified	98.2	4.7	1.2	2.0	0.76	3.7
	retopology	99.6	2.4	0.4	1.1	0.45	0.2

Table 4: FEA results as mean stress (μ), standard deviation (σ) and deviation from reference (100 MPa) for all the surveyed models. The aspect ratio for each mesh is expressed in terms of mean (μ), standard deviation (σ) and percentage of element that exceed the value of 3

The FEAs have been run for each model and the normal stress along the load's direction has been registered. Figure 13 shows the results for the 3 models originated from Minolta scans. As expected, all the three models present a non-uniform and non-constant distribution of the stress. It can be ascribed to the noise introduced by the laser scanner and, to the fact that the cross-section is not perfectly 2500mm^2. However, the retopologized model presents a stress distribution that is less sparse than the other two. The range of normal stress of the retopologized model is more close to the true value (100 MPa): this is a sign that the initial mesh, in this case, leads to better FEA results. Figure 13a and Figure 13b present also pronounced peaks of stress, while this phenomenon is less evident in Figure 13c: local singularities are responsible for those. In fact, the results of the analysis is strongly affected by artifacts that spots the model surfaces (Figure 14): these areas are also the one where the aspect ration of the element increase, leading to unreliable stress values. Furthermore, due to a more uniform mesh, the retopologized model has been handled easier and more efficiently by the FEA software. The as-is model was hard to mesh due to its high resolution mesh. Even with a so simple geometry, the FEA software lasts long time in order to complete the mesh without gaining any advantage over the other two models.

Similar patterns have been observed for the other technologies in this survey and, the same considerations can be done. Furthermore, the peaks of stress introduced by the artifacts could lead to misinterpretation of the stress distribution when presented by stress contours. For these reasons, Table 4 reports the results looking at the stress distribution in terms of average value and standard deviation. Deviation from the nominal value is reported as well. Considering the average values, the results are quite satisfactory for all the models since the maximum deviation from the analytic results is 2.3 % in the worst case, represented by the Minolta laser scanner: sharp edge detection and reconstruction with this device was in fact the most problematic. As can be notice from Fig.13, most of the stress concentrations are close to the edges. The standard deviations can be seen as a metric of the number of defects meshes are affected of. The three retopologized models lead to lower standard deviation with all the devices, symptoms of less number of artifacts. This trend is also confirmed by the better aspect ratio values of the retopologized models. Retopology compels the mesh to be

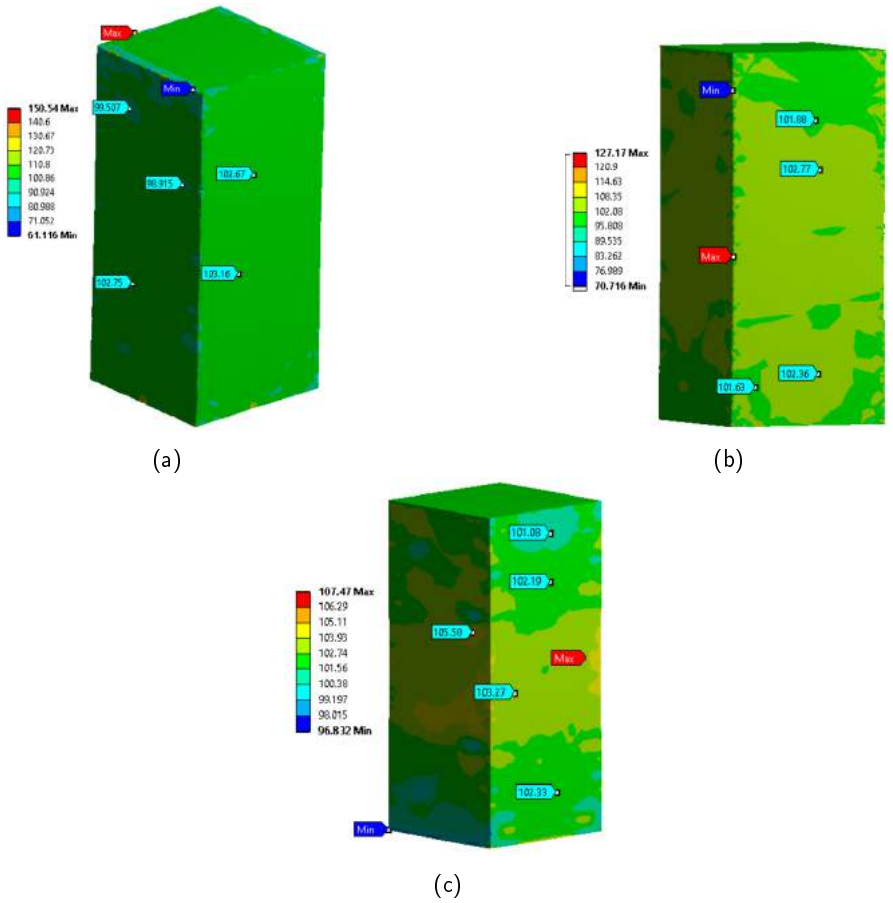

Figure 13: Normal stress contour expressed in MPa for the models originated from Minolta: (a) As-Is tessellated surface; (b) Triangular simplification; (c) Retopology.

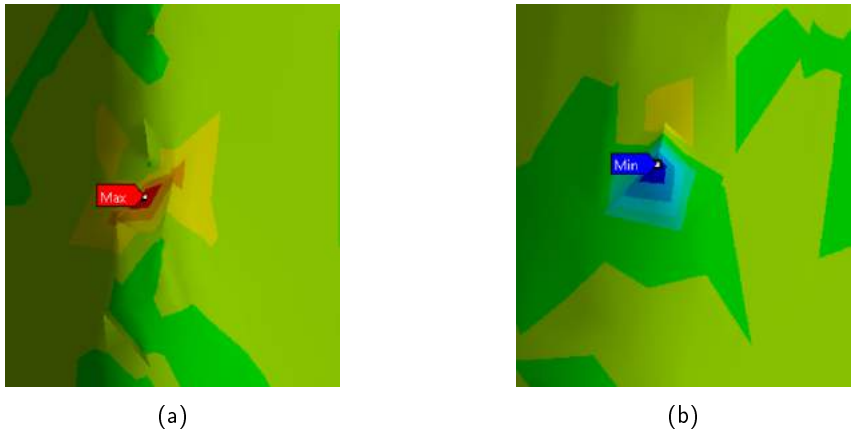

Figure 14: Normal stress contour expressed in MPa for the models originated from Minolta: (a) zoom on the max; (b) zoom on the min.

more uniform, hence effectively more suitable for FEA. The standard deviation resulting from the next engine device are higher than others, probably due to the technical specifications of the device: in the acquisition phase some problems have occurred in detecting the entire surface.The trend of the aspect ration confirm these consideration: the retopologized models offers a mesh with much lower aspect ratio.

6 CONCLUSION

This work investigates how tessellated surface originated from reality-based survey techniques affect the generation of computational grid for FEA and the related results. A benchmark specimen (i.e. 50x50x120 mm steel parallelepiped) has been used in order to provide quantitative outcomes and keep under full control the whole pipeline. As-is scanned tessellated surface reconstruction leads to high resolution models: high number of triangles can lead to unsuitable and heavy tessellated surface, difficult to be converted in a computational grid. The decimation process is a mandatory step in order to have a tessellated surface suitable to be converted in a volumetric model for FEA. The triangular simplification (i.e. Vertex Decimation) reduces the number of triangle but a degradation of the mesh quality (i.e. aspect ration) is one of the drawback, possibly leading to inaccurate FEA results. Even if retopology adds a smoothing on the simplified tessellated surface, the reorganization of the quadrangular elements on the surface avoids sharp artifacts, non-manifold edges and permits a simplification of the model keeping the accuracy unchanged and guaranteeing a good FE mesh quality as well. The combined effect of decimation and feature-preservation capabilities of the instant field-aligned algorithm makes it one of the best candidate to streamline the use of reality-based model for FEA. The drawback of the retopology, at least for the implementation adopted in this work, does not allow intelligent and adaptive refinement. The uniform distribution of elements on planar regions is unuseful and, from a FE perspective, it could lead to computational problem in presence of strong field gradient or complex surfaces. Another issue that Instant Meshes software does not allow to set a fixed number of superficial elements for the final, simplified tessellated surface. The software suggests, by default, the parameters to be applied to the simplification process starting from the accuracy of the (estimated) high resolution tessellated surface.

All the three models, in terms of estimated stress, gave acceptable results. The presence of artifacts and noise alter the local behavior (peaks of stresses) while the global stress distribution is just slightly affected (the mean stress is close to the analytic solution). Hence, if we are interested in the global behaviour of a structure (i.e. buildings, monuments and so on), this general purpose structure seems appropriate to obtain reliable FE results. Whereas if the scale of the phenomena we are interested in is small, the general purpose pipeline adopted here is not suitable.

The accuracy of the acquisition, derived from the uncertainty or the precision of the technology used, plays a crucial role along the whole pipeline. In this work, the photogrammetric acquisition appears to be more accurate that the one performed with laser devices, even if they have better technical specifications and are considered usually more accurate. The reason is that the photogrammetric process is less affected by the presence of sharp edges due to its very nature. Given that the major local deviations (artifacts) from the nominal geometry are along the edges, the result of the comparison (Table 2) shows that the SfM models is the closest to the nominal geometry. This is just for the specific case of the parallelepiped and any generalization of this fact is not proper.

Findings of our research can be summarized as follow: (i) laser scanners still lacks on detecting sharp edges (essential for most engineering product), consequently they are one of the greatest source of geometrical error; (ii) SfM, on the contrary, showed a high performance in creating a proper models ready to be simplified; (iii) simplification and retopology do not introduce excessive geometric approximations but considerable advantages in the FEA mesh generation; and (iv) geometric inaccuracies (i.e. irregular surface that should be planar face instead and sharp edges) is reflected in inaccurate FEA results, mostly caused by inaccurate application of boundary conditions and loads in addition to the geometric approximation. Moreover, meshing the retopologized models is easier because their tessellation is uniform and smooth. For simple geometry like our case

study is, the meshing with hexahedra has been straightforward while with the other tessellation has not been even possible. The unique characteristics of the retopologized model likely help meshing procedures in case of complex shapes as well. Also, aforementioned advantages affects the application of loads and boundary conditions that ends up to be easier. It has to be pointed out that, this work does not allow to make any general conclusion about the optimal pipeline, especially on the point (ii) aforementioned.

As future work, the benchmark will be surveyed with a structured light device that is supposed to provide more accurate results especially regarding sharp edges. In this way, the artifacts discovered on the final high resolution tessellated surface are supposed to be avoided. The idea is to analyze pro and cons of each technique, to find the best to be used for the survey of manufacturing objects, then exposed to FEA. Furthermore, the make the results more general and to derive the optimal pipeline, more complex objects should be surveyed, always knowing the exact or experimental stress distribution to make the comparison systematic and reliable.

ORCID

Marco Rossoni, http://orcid.org/0000-0003-2714-9043
Sara Gonizzi Barsanti, http://orcid.org/0000-0002-7650-1616
Giorgio Colombo, http://orcid.org/0000-0002-9999-8960
Gabriele Guidi, http://orcid.org/0000-0002-8857-0096

REFERENCES

[1] Adhikary, N.; Gurumoorthy, B.: A slice-based algorithm for automatic and feature-preserving hole-filling in a CAD mesh model. Computer-Aided Design and Applications, 15(6), 780–795, 2018. http://doi.org/10.1080/16864360.2018.1466807.

[2] Attene, M.; Campen, M.; Kobbelt, L.: Polygon mesh repairing. ACM Computing Surveys, 45(2), 1–33, 2013. http://doi.org/10.1145/2431211.2431214.

[3] Berger, M.; Tagliasacchi, A.; Seversky, L.M.; Alliez, P.; Levine, J.A.; Sharf, A.; Silva, C.T.: State of the art in surface reconstruction from point clouds. In Eurographics 2014 - State of the Art Reports, 2014. http://doi.org/10.2312/egst.20141040.

[4] Bommes, D.; Lévy, B.; Pietroni, N.; Puppo, E.; Silva, C.; Tarini, M.; Zorin, D.: Quad-mesh generation and processing: A survey. Computer Graphics Forum, 32(6), 51–76, 2013. http://doi.org/10.1111/cgf.12014.

[5] Bommes, D.; Zimmer, H.; Kobbelt, L.: Mixed-integer quadrangulation. ACM Transactions on Graphics, 28(3), 1, 2009. http://doi.org/10.1145/1531326.1531383.

[6] Botsch, M.; Kobbelt, L.; Pauly, M.; Alliez, P.; Levy, B.: Polygon Mesh Processing. A K Peters/CRC Press, 2010. http://doi.org/10.1201/b10688.

[7] Buonamici, F.; Carfagni, M.; Furferi, R.; Governi, L.; Lapini, A.; Volpe, Y.: Reverse engineering modeling methods and tools: a survey. Computer-Aided Design and Applications, 15(3), 443–464, 2017. http://doi.org/10.1080/16864360.2017.1397894.

[8] Buonamici, F.; Carfagni, M.; Furferi, R.; Governi, L.; Lapini, A.; Volpe, Y.: Reverse engineering of mechanical parts: A template-based approach. Journal of Computational Design and Engineering, 5(2), 145–159, 2018. http://doi.org/10.1016/j.jcde.2017.11.009.

[9] Burkhart, T.A.; Andrews, D.M.; Dunning, C.E.: Finite element modeling mesh quality, energy balance and validation methods: A review with recommendations associated with the modeling of bone tissue. Journal of Biomechanics, 46(9), 1477–1488, 2013. http://doi.org/10.1016/j.jbiomech.2013.03.022.

[10] Castellazzi, G.; D'Altri, A.; Bitelli, G.; Selvaggi, I.; Lambertini, A.: From laser scanning to finite element analysis of complex buildings by using a semi-automatic procedure. Sensors, 15(8), 18360–18380, 2015. http://doi.org/10.3390/s150818360.

[11] Cignoni, P.; Callieri, M.; Corsini, M.; Dellepiane, M.; Ganovelli, F.; Ranzuglia, G.: MeshLab: an Open-Source Mesh Processing Tool. In Eurographics Italian Chapter Conference, 2008. http://doi.org/10.2312/LocalChapterEvents/ItalChap/ItalianChapConf2008/129-136.

[12] Comotti, C.; Regazzoni, D.; Rizzi, C.; Vitali, A.: Additive manufacturing to advance functional design: An application in the medical field. Journal of Computing and Information Science in Engineering, 17(3), 031006, 2017. http://doi.org/10.1115/1.4033994.

[13] Floriani, L.D.: A pyramidal data structure for triangle-based surface description. IEEE Computer Graphics and Applications, 9(2), 67–78, 1989. http://doi.org/10.1109/38.19053.

[14] Franc, M.: Methods for Polygonal Mesh Simplification. Ph.D. thesis, University of West Bohemia, 2002.

[15] Geng, Z.; Bidanda, B.: Review of reverse engineering systems – current state of the art. Virtual and Physical Prototyping, 12(2), 161–172, 2017. http://doi.org/10.1080/17452759.2017.1302787.

[16] Gonizzi Barsanti, S.; Guidi, G.: A geometric processing workflow for transforming realit-based 3D models in volumetric meshes suitable for fea. ISPRS - International Archives of the Photogrammetry, Remote Sensing and Spatial Information Sciences, XLII-2/W3, 331–338, 2017. http://doi.org/10.5194/isprs-archives-XLII-2-W3-331-2017.

[17] Gonizzi Barsanti, S.; Remondino, F.; Fernández-Palacios, B.; Visintini, D.: Critical factors and guidelines for 3D surveying and modelling in cultural heritage. International Journal of Heritage in the Digital Era, 3,(1), 141–158, 2014. http://doi.org/10.1260/2047-4970.3.1.141.

[18] He, Y.; Liang, B.; Yang, J.; Li, S.; He, J.: An iterative closest points algorithm for registration of 3D laser scanner point clouds with geometric features. Sensors, 17(8), 1862, 2017. http://doi.org/10.3390/s17081862.

[19] Hoppe, H.: Progressive meshes. In Proceedings of the 23rd annual conference on Computer graphics and interactive techniques - SIGGRAPH '96. ACM Press, 1996. http://doi.org/10.1145/237170.237216.

[20] InstantMesh: https://github.com/wjakob/instant-meshes. [Online; accessed 30-March-2019].

[21] Jakob, W.; Tarini, M.; Panozzo, D.; Sorkine-Hornung, O.: Instant field-aligned meshes. ACM Transactions on Graphics, 34(6), 1–15, 2015. http://doi.org/10.1145/2816795.2818078.

[22] Kazhdan, M.; Hoppe, H.: Screened poisson surface reconstruction. ACM Transactions on Graphics, 32(3), 1–13, 2013. http://doi.org/10.1145/2487228.2487237.

[23] Luhmann, T.; Robson, S.; Kyle, S.; Boehm, J.: Close-Range Photogrammetry and 3D Imaging. De Gruyter, Berlin, Germany, 2014. http://doi.org/10.1201/b10688.

[24] Mikhail, E.; Bethel, J.; McGlone, J.: Introduction to Modern Photogrammetry. John Wiley & Sons Inc., New York, 2001. ISBN 978-0-471-30924-6.

[25] Raja, V.: Introduction to reverse engineering. In Reverse Engineering: An Industrial Perspective, 2008. http://doi.org/10.1007/978-1-84628-856-2_1.

[26] Schroeder, W.J.; Zarge, J.A.; Lorensen, W.E.: Decimation of triangle meshes. ACM SIGGRAPH Computer Graphics, 26(2), 65–70, 1992. http://doi.org/10.1145/142920.134010.

[27] Taime, A.; Saaidi, A.; Satori, K.: Comparative study of mesh simplification algorithms. In Lecture Notes in Electrical Engineering, 2016. http://doi.org/10.1007/978-3-319-30301-7_30.

[28] Taubin, G.: Curve and surface smoothing without shrinkage. In Proceedings of IEEE International Conference on Computer Vision, 1995. http://doi.org/10.1109/iccv.1995.466848.

[29] Wang, J.; Gu, D.; Yu, Z.; Tan, C.; Zhou, L.: A framework for 3D model reconstruction in reverse engineering. Computers & Industrial Engineering, 63(4), 1189–1200, 2012. http://doi.org/10.1016/j.cie.2012.07.009.

[30] Westoby, M.; Brasington, J.; Glasser, N.; Hambrey, M.; Reynolds, J.: 'structure-from-motion' photogrammetry: A low-cost, effective tool for geoscience applications. Geomorphology, 179, 300–314, 2012. http://doi.org/10.1016/j.geomorph.2012.08.021.

[31] White, S.: Virtual archaeology - the NextEngine desktop laser scanner. Archaeology International, 18(0), 41, 2015. http://doi.org/10.5334/ai.1804.